

Journal of Materials Chemistry B

Accepted Manuscript



This is an *Accepted Manuscript*, which has been through the Royal Society of Chemistry peer review process and has been accepted for publication.

Accepted Manuscripts are published online shortly after acceptance, before technical editing, formatting and proof reading. Using this free service, authors can make their results available to the community, in citable form, before we publish the edited article. We will replace this *Accepted Manuscript* with the edited and formatted *Advance Article* as soon as it is available.

You can find more information about *Accepted Manuscripts* in the [Information for Authors](#).

Please note that technical editing may introduce minor changes to the text and/or graphics, which may alter content. The journal's standard [Terms & Conditions](#) and the [Ethical guidelines](#) still apply. In no event shall the Royal Society of Chemistry be held responsible for any errors or omissions in this *Accepted Manuscript* or any consequences arising from the use of any information it contains.



Fetuin-A Adsorption and Stabilization of Calcium Carbonate Nanoparticles in a Simulated Body Fluid

Erick S. Vasquez^a, Janice L. Cunningham^b, Justin B. McMahan^b, C. LaShan Simpson^b, and Keisha B. Walters^{a*}

Received 00th January 20xx,
Accepted 00th January 20xx

DOI: 10.1039/x0xx00000x

www.rsc.org/

Fetuin-A is a serum glycoprotein identified as a calcification inhibitor, and a key player in bone formation and human metabolic processes. A study on binding mechanisms of Fetuin-A with calcium carbonate nanoparticles in a simulated body fluid (DMEM) environment is presented. Observed interactions between Fetuin-A and the CaCO₃ nanoparticles reveal an initial adsorption process, followed by a stabilization stage, and then a solubilization period for the Fetuin-A/CaCO₃ complex. FTIR and XPS are used to monitor functional group and elemental composition changes during the initial adsorption process between Fetuin-A and the CaCO₃ nanoparticles. Distinctive Fetuin-A/CaCO₃ complex structures—also known as mineralo-protein particles—are imaged with TEM and SEM. DLS and UV-Vis methods are used to further characterize the *in situ* binding mechanisms. Results of this study can guide the design of complex organic-inorganic hybrid materials, improve current drug delivery methods, and provide insight in monitoring and controlling interactions between Fetuin-A and external calcium ions.

1. Introduction

Composites where the individual materials have micro-to-nano length scales have demonstrated many advantages over single-material synthetic materials, including properties such as biocompatibility, stability, dispersion, and surface-functionalities that can be manipulated and enhanced.¹⁻⁴ For example, biocomposites—inorganic materials combined with proteins, natural polymers, or other biomolecules—display greater biocompatibility than solely inorganic, synthetic materials.⁵ Furthermore, small length scales of the composite components supports the mimicking of natural mechanisms which occur in the formation of organic biocomposites (e.g., crustaceans, shell-fish, skeletal bone).⁴⁻⁸ Moving beyond the realm of 'bioinspired' to the development of novel 'self-functioning' materials, which utilize inherent chemical and biological mechanisms to carry out specific functions, allows for enhanced dynamic processes such as self-assembly, reversible adsorption/desorption, and solids precipitation and resolubilization to occur.⁹⁻¹¹

This work examines biomineral formation and remodeling; specifically focusing on the role of proteins on stabilizing the

formation and solubilization of calcium nanoparticles. Key players in the skeletal biomineralization process have been shown to also play a significant role in the development of pathological vascular calcification.¹² For instance, proteins regulate bone growth and remodeling by actively inhibiting or promoting mineral deposition and cell mediated activities. These regulatory mechanisms may be effective at treating vascular calcification given its similarity to bone biomineralization.¹³ Additionally, an understanding of the interactions between proteins and mineral nuclei is necessary for the development of protein-nanoparticle therapies that can effectively treat and potentially reverse vascular calcification. For example, protein-mineral interactions observed in biomineralization have been utilized to design novel nanoparticle-protein adsorption techniques for the development of drug delivery systems, theranostic procedures, and gene therapy for the transport of biological macro-molecules into cells and tissues.¹⁴⁻¹⁶ The important role of acidic proteins in the structure and mineralization of calcified tissues has long been recognized; however, the relationship between proteins and their precise function in (de)mineralization processes remains obscure.¹⁷ Fetuin-A, also known as α -2-Heremans Schmid glycoprotein (AHS2G), is a well-studied acidic serum glycoprotein and physiological regulator of bone metabolism. Many studies suggest that Fetuin-A acts as a chaperone protein that produces and stabilizes calcium phosphate mineral colloids, also referred to as calciprotein particles (CPPs) or fetuin mineral complexes (FMCs).¹⁸ Once formed, Fetuin-A facilitates cellular resorption of CPPs; however, the exact mechanism(s) of CPPs clearance from cells has yet to be determined.^{19, 20} In

^a Dave C. Swalm School of Chemical Engineering, Mailstop 9595, 330 Swalm Chemical Eng. Bldg., Mississippi State, MS, 39762, USA. E-mail: kwalters@che.msstate.edu

^b Agricultural and Biological Engineering Department, Mailstop 9632, 130 Creelman St., Mississippi State, MS, 39762, USA

^c Electronic Supplementary Information (ESI) available: [ESI1. Infrared spectroscopic analysis of CaCO₃ nanoparticles and Fetuin-A; ESI2. Time-dependent study of Fetuin-A/CaCO₃ complexes; ESI3. UV-Vis Absorbance of Fetuin-A, CaCO₃ particles, and Fetuin-A/CaCO₃ complexes.]. See DOI: 10.1039/x0xx00000x

order to further elucidate the exact mechanism of Fetuin-A inhibition and stabilization of mineral colloids, several groups have studied the ability of Fetuin-A to form CPPs under supersaturated concentrations of calcium and phosphate *in vivo* and *in vitro*. For example, Heiss *et al.* used scanning electron microscopy (SEM) to show that the addition of miniscule amounts of Fetuin-A/AHSG induced morphological changes in basic calcium phosphate precipitations that resulted in a brittle appearance of the precipitate formed.¹⁸ Pasch *et al.* used three-dimensional cross correlation dynamic light scattering (DLS) to show that CPP formation is a time dependent biphasic process which results in morphological changes as well as an increased CPP diameter.²¹ Lastly, the formation and stability kinetics of the CPPs, analyzed using time-resolved dynamic light scattering, showed CPP size and that the secondary ripening transition phase depends more on Fetuin-A/mineral concentration ratio than reaction temperature.²²

Fetuin-A interaction and stabilizing ability with calcium phosphate is a well-known phenomenon; as such, the interest of this study is to observe whether Fetuin-A is a potent enough regulator of mineralization to control aggregation and growth of other types of calcium polymorphs. To date, there have been no experimental studies on Fetuin-A's ability to stabilize other sources of calcium, including calcium carbonate (CaCO_3) which has gained tremendous interest as a stabilizer for drug delivery applications.^{23,24} Moreover, CaCO_3 biocompatibility and biodegradability has led to the development of different structures such as self-assembled nanovesicles,²³ protein adsorption/release experiments,²⁴ and the development of hollow microspheres.²⁵

CaCO_3 crystalline forms (i.e. calcite, valerite, and aragonite) are usually obtained from an amorphous calcium carbonate (ACC) precursor which is a naturally occurring composite extensively studied during biomineralization in living organisms.²⁴ ACCs are also used as a template for core-shell particles,^{26,27} but are thermodynamically unstable and tend to crystallize. However, researchers have discovered that in some instances transient biogenic ACC has the ability to remain stable for the entire life span of some organisms (e.g., exoskeleton shells of crustaceans).²⁶ In particular, this work pursues to obtain a better understanding of Fetuin-A adsorption, stabilization, and solubilization of CaCO_3 crystals in the presence of a simulated body fluid in order to develop a protein/nanocomposite-based therapy for drug delivery applications, and to motivate further studies for possible competing effects with the well-known CPPs.

This study focuses on the binding mechanisms of Fetuin-A, a model protein for the further understanding of acidic proteins, with CaCO_3 nanoparticles. As biomineralization naturally occurs under supersaturated extracellular environments and in the presence of ions we wanted to study Fetuin-A interaction with mineral particles in a setting that would mimic a real-life biological system (i.e. blood) as closely as possible. To better understand the *in vivo* bioactivity of the Fetuin-A protein as it stabilizes and binds CaCO_3 particles we utilized Dulbecco's Modified Eagle's Medium (DMEM) as a simulated body fluid.²⁹⁻

³¹ The overall objective of this investigation is to characterize the binding mechanisms and chemical interactions between Fetuin-A and calcium-based nanoparticles in a simulated body fluid. Specific findings presented include: (1) elucidation of the role of Fetuin-A as a model stabilizer of calcium-mineral polymorphs, including confirmation of protein adsorption and binding with CaCO_3 nanoparticles; (2) reporting, for the first time, infrared spectroscopic spectral signatures of Fetuin-A and the chemical changes when binding with CaCO_3 nanoparticles; (3) identification of morphological changes in these Fetuin-A/ CaCO_3 nanoparticle complexes after formation; and (4) validation of protein monolayer adsorption onto CaCO_3 surfaces and solubilization over time utilizing *in situ* dynamic light scattering and spectroscopic methods to assess protein adsorption and time-dependent binding onto CaCO_3 nanoparticles.

2. Results and Discussion

2.1 Chemical Characterization of Fetuin-A, CaCO_3 , and Fetuin-A/ CaCO_3 nanoparticle complexes

The "as-received" CaCO_3 nanoparticles and pure Fetuin-A protein were characterized using attenuated total reflection FTIR (ATR-FTIR) spectroscopy to evaluate the infrared absorption bands corresponding to their chemical composition. CaCO_3 crystalline or amorphous state has been previously characterized using FTIR, as discussed elsewhere.³²⁻³⁴ In this study, the "as-received" CaCO_3 nanoparticles were characterized with ATR-FTIR and three distinctive absorption peaks were observed. We have confirmed the presence of calcite, in its purest form, in the CaCO_3 nanoparticles used in this study due to the appearance of the absorption bands at 1426 cm^{-1} , 876 cm^{-1} and 712 cm^{-1} wavenumbers (Figs. 1A and S1) corresponding to calcite stretching vibrations (ν_3 , ν_2 , and ν_4 , respectively).³²⁻³⁴ A complete spectrum, collected with a separate FTIR detector, is shown and discussed in ESI 1.

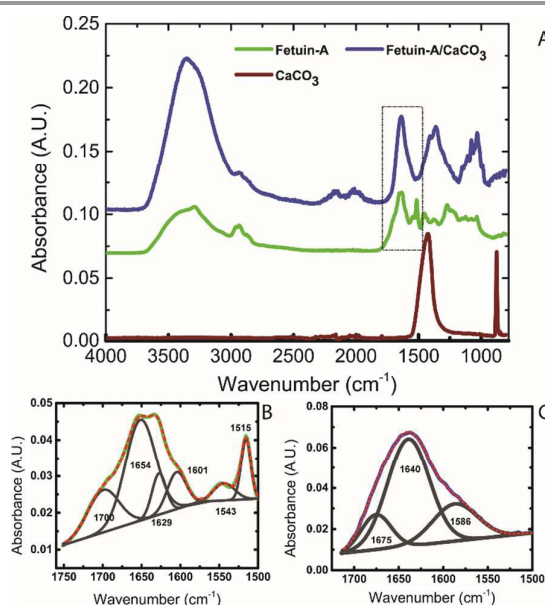


Figure 1. ATR-FTIR spectra for (A) Fetuin-A, CaCO₃, and Fetuin-A/CaCO₃ complexes, (B) Amide-I and Amide-II region for neat Fetuin-A, and (C) Amide-I and Amide-II region showing absorption changes after the complexation of Fetuin-A with CaCO₃.

Similar characterization was performed on neat Fetuin-A and is, to the authors' knowledge, the first study reporting the infrared (IR) molecular absorptions of this glycoprotein (Fig. 1A; Fig. S2). Typically, IR characterization of proteins is performed by deconvoluting the amide I and amide II regions of the IR spectrum.³⁵ This section focuses on the main differences between Fetuin-A and Fetuin-A/CaCO₃ through an analysis of the amide I and II spectral region (Fig. 1B,C). A full discussion of the characteristics bands of Fetuin-A is provided in ESI 1,(Fig. S2, Table S1).

For neat Fetuin-A, the amide I region shows four distinctive peaks between 1600-1700 cm⁻¹ (Fig. 1B). Two peaks corresponding to the C=O stretching vibrations were observed at 1700 cm⁻¹ and at 1654 cm⁻¹, respectively. The peak at 1700 cm⁻¹ is attributed to the presence of glutamic acid or asparagine aminoacids.³⁶ The peaks observed at 1654 cm⁻¹ in the amide I region can be assigned to an α -helix (1654 cm⁻¹) secondary protein structure and/or to the C=O stretching vibrations from arginine aminoacids.³⁶ Peaks for β -sheet (1629 cm⁻¹) secondary structures^{35, 36} intermolecular β -sheets turns (1601 cm⁻¹)³⁵ were observed for neat Fetuin-A. Significant spectral changes were observed after the addition of Fetuin-A to the CaCO₃ nanoparticles.

For the Fetuin-A/CaCO₃ nanoparticle complex only three absorption peaks were observed, indicating binding induced changes in the chemical structure. Similar conformational changes of protein adsorption on nanoparticles using FTIR have been reported for other protein types.^{37, 38} For the characteristic amide I vibrations, only two peaks were identified for Fetuin-A/CaCO₃; located at 1640 cm⁻¹ and 1675 cm⁻¹ these peaks correspond to asparagine (C=O) amino acid groups.³⁶ This result points to a potential mechanism for Fetuin-A adsorption onto the CaCO₃ particles, specifically involvement of the β -sheets and α -helix turns of the protein as indicated by the loss of these amide I peaks in spectra for the Fetuin-A/CaCO₃ complexes. This result indicates that the acidic residues on the β -sheet structure of Fetuin-A are responsible for calcium inhibition and adsorption of the protein onto this calcium substrate, as previously discussed by Heiss *et al.*¹⁸

The amide II band for neat Fetuin-A shows an absorption peak at 1543 cm⁻¹ (N-H) corresponding to a primary amine deformation.³⁶ Another peak located at 1515 cm⁻¹ was also observed, and this peak can be assigned to C-O stretching in the alcohols of amino acids, such as tyr-OH or *p*-cresol (Fig. 1C).^{36, 39} When Fetuin-A was combined with CaCO₃ particles, a significant shifting of the amide II peak was observed (1586 cm⁻¹); this significant increase in wavenumber is attributed to the adsorption interactions between Fetuin-A and the CaCO₃ nanoparticles.⁴⁰

Surface coverage and elemental compositions was studied using X-ray photoelectron spectroscopy (XPS) for both the "as-received" CaCO₃ nanoparticles and the Fetuin-A/CaCO₃ complexes. Fig. 2A displays representative survey scans for CaCO₃ nanoparticles and Fetuin-A/CaCO₃ complexes.

Elemental surface composition for the CaCO₃ nanoparticles included carbon (C, 32.8 \pm 3.1), calcium (Ca, 18.4 \pm 3.8%), and oxygen (O, 48.9 \pm 0.9%). Moreover, these atomic percentages are close to the theoretical atomic elemental composition of CaCO₃ (20% C, 20% Ca, and 60% O), confirming the presence of CaCO₃ as previously shown by IR analysis. The higher carbon content observed in CaCO₃ nanoparticles is attributed to adventitious carbon present in XPS measurements when materials are exposed to air.⁴¹ To further investigate the atomic percentage of calcium, SEM-EDS was performed and an average value of 22.8 \pm 13.2% was reported.

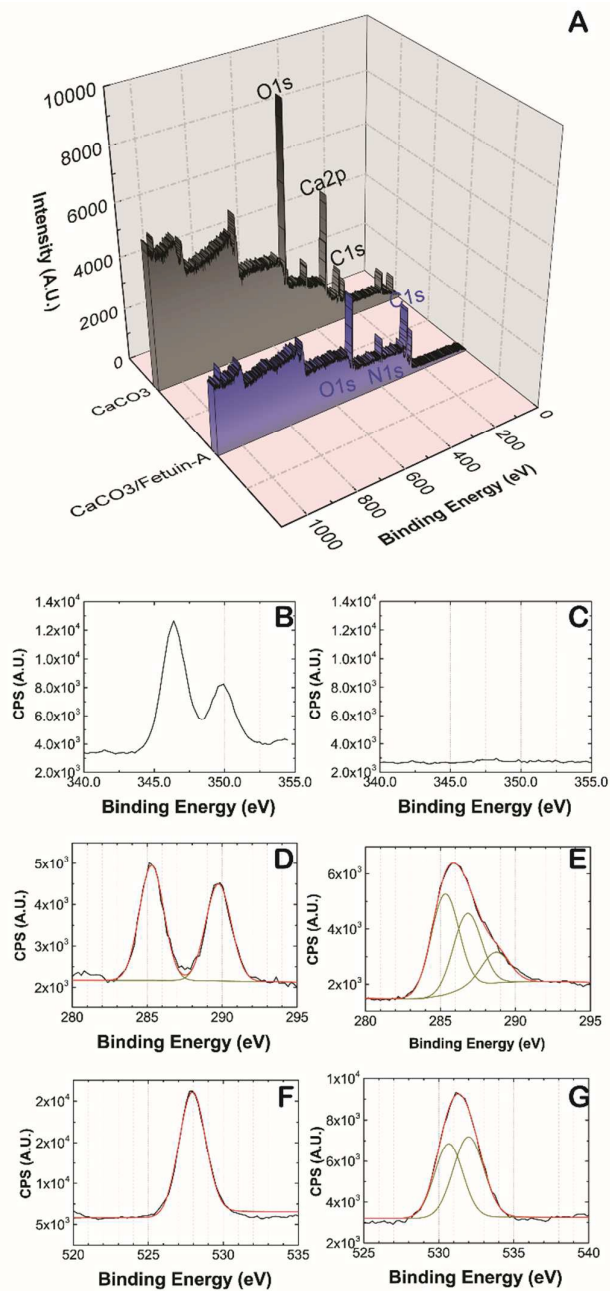


Figure 2. (A) XPS survey scans confirming the addition of the serum glycoprotein Fetuin-A onto the surface of the CaCO₃ nanoparticle aggregates, as shown by the presence of nitrogen. Comparison of the high-resolution calcium, carbon, and oxygen scans for the neat CaCO₃ particles (B,D,F) and Fetuin-A/CaCO₃ complexes (C,E,G) show complete coverage of the CaCO₃ surface with Fetuin-A and protein-mineral binding. Nitrogen high resolution XPS scans are shown in Figure S5.

Elemental compositions for the Fetuin-A/CaCO₃ complexes were also measured and compared with XPS and SEM-EDS results. The average atomic composition reported by XPS for Fetuin-A/CaCO₃ was 61.4 ± 0.6% C, 31.3 ± 0.8% O, and 7.3 ± 1.5% N. The presence of nitrogen and the increase in the carbon content, despite the presence of adventitious carbon, correlates with the inclusion of glycoproteins, confirming the presence of Fetuin-A on the surface of CaCO₃ nanoparticles.³⁹ Moreover, after Fetuin-A adsorption, the presence of calcium could not be detected within the 10 nm penetration depth of XPS suggesting that CaCO₃ has been completely covered by a layer of Fetuin-A, a Fetuin-A/CaCO₃ complex structure that would result in CaCO₃ particle stabilization. Similarly, SEM-EDS results showed a negligible atomic percentage for Ca of 0.06 ± 0.11%, validating the surface coverage of Fetuin-A on the CaCO₃ nanoparticles.

High-resolution XPS identified specific functional groups and chemical bonds present as part of the chemical changes due to the formation of the Fetuin-A/CaCO₃ complex. Fig. 2B,C show the high resolution calcium scans for CaCO₃ and the Fetuin-A/CaCO₃ complex. For the neat CaCO₃ sample, two distinctive calcium peaks were observed at 246.5 and 250.0 eV, corresponding to the Ca 2p_{3/2} and Ca 2p_{1/2} photoelectron lines, respectively.^{42,43} After Fetuin-A adsorption, these Ca peaks were no longer observed (Fig. 2C), demonstrating protein surface adsorption. High resolution carbon and oxygen scans were also performed (Fig. 2D-G), and adsorption-related C and O transitions observed. The C 1s peak corresponding to C-C/C-H bonds was observed in both samples at 285.3 eV corresponding to the carbon present in Fetuin-A, and this photoelectron line was used as a reference calibration for charge compensation.⁴⁴ An additional peak was observed at approximately 290 eV in the CaCO₃ sample (Fig. 2D), confirming the presence of the carbonate ((C-O)₃) group.⁴²

Fetuin-A adsorption resulted in a number of additional C and O absorption peaks. The presence of the Fetuin-A glycoprotein on the CaCO₃ particles was demonstrated by the peak at 285.3 eV assigned to C-C/C-H bonds found in carbohydrates, proteins, lipids and hydrocarbon chains.^{40,45} Additionally, the peak at 286.8 eV can be attributed to C-O, C-N and/or N-C-O bonds.^{40,46} A second peak located at 288.7 eV corresponds to the carbon of an amide functional group (N-C=O), which is present in the Fetuin-A glycoprotein.^{46,47} Lastly, results for the O 1s high-resolution XPS analysis on the CaCO₃ nanoparticles revealed a 528 eV binding energy attributable to the oxygen ((C-O)₃) in CaCO₃.⁴³ Due to Fetuin-A adsorption in forming the Fetuin-A/CaCO₃ complex, two distinctive chemical shifts were observed. The peak observed at 530.6 eV is assigned to oxygen in amino acid chains,⁴⁸ and the peak observed at 532 eV is assigned to a C=O peptide bond,⁴⁵ or possibly to residual -OH bonds after evaporation of the Dulbecco's modified Eagle's medium (DMEM).⁴⁹ Moreover, the presence of an N 1s photoelectron line confirms Fetuin-A is present on the exterior

of the Fetuin-A/CaCO₃ complexes (additional details in Fig. S3).⁴⁵ These XPS data corroborate the ATR-FTIR results in confirming the presence of Fetuin-A on the exterior of the Fetuin-A/CaCO₃ complex.

2.2 Morphological Characterization of Fetuin-A, CaCO₃, and Fetuin-A/CaCO₃ complexes.

The formation of organic/inorganic composites involves changes in crystal morphology and shape, with structural conformations and conditions to control changes in structure yet to be explored.⁵⁰ Fetuin-A when combined with calcium phosphate particles can produce calciprotein particles or fetuin-mineral complexes, as reported elsewhere.^{18, 22, 51-53} In terms of morphological characterization, calciprotein particles are soluble colloidal spheres stabilized by the presence of Fetuin-A; however, formation of large precipitates (~ 450 nm) with radially expanded, oriented crystalline needles has been shown as a function of time.¹⁸ Morphology of complexed Fetuin-A is important, as the structure impacts the ability to adsorb and desorb complexed minerals. Thus, while Fetuin-A has shown to act as an inhibitor of ectopic calcification, in order for Fetuin-A to selectively complex with vascular calcification the requisite complexed protein morphology(s) need to be investigated further.^{22, 54}

Small-angle neutron scattering data has shown that Fetuin-A does not inhibit mineral nucleation but does prevent growth and aggregation of mineral particles by covering with a layer of Fetuin-A.⁵⁵ In an effort to obtain a better understanding of the morphological structural changes of the Fetuin-A/CaCO₃ complexes, SEM and TEM characterization was performed. Analysis of the CaCO₃ particles by SEM shows a rhombohedral morphological structure (Fig. 3). Calcite crystals with a rhombohedral shape have also been reported elsewhere, confirming the crystal structure of the 'as-received' CaCO₃ nanoparticles.⁵⁶ Aggregation of CaCO₃ particles without any stabilizer present in solution was observed as the particle solution was dried on the SEM grid (Fig. 3A inset). The CaCO₃ particles were also investigated using TEM as shown in Fig. 4. The presence of densely packed clusters and aggregation of CaCO₃ was observed (Fig. 4A,B).

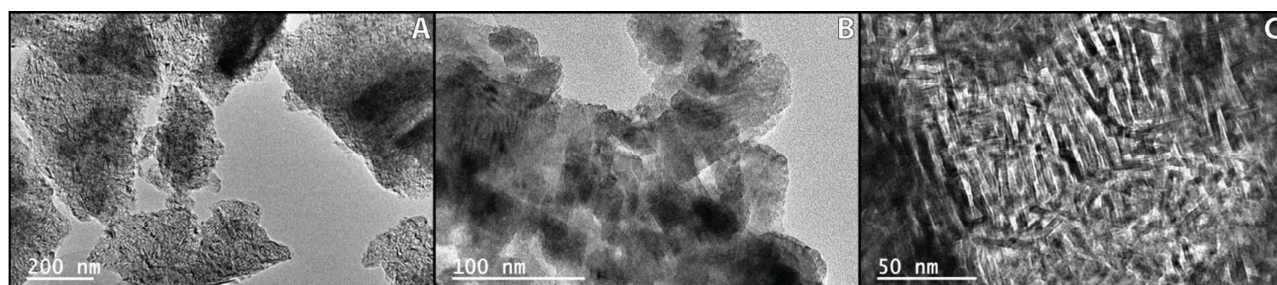


Figure 4. TEM images of CaCO_3 showing aggregation (A,B). At high resolution, a rhombohedral-like structure is observed which is characteristic of calcite materials (C).



Figure 3. SEM image of neat calcium carbonate nanoparticles demonstrating a rhombohedral crystalline structure and nanoparticle aggregation. Inset image confirms the presence of non-uniform CaCO_3 particles. Scale bars on the main and inset images represent 10 microns.

Rhombohedral structures can also be seen with TEM at higher magnifications (Fig. 4C) for the precipitated CaCO_3 particles, confirming the presence of nanosized CaCO_3 crystals within a larger-scale aggregated structure. These results match those in prior studies on aggregation of the mineral phase.⁵⁷ Furthermore, DLS studies are shown to confirm the aggregation of the CaCO_3 crystals while in DMEM solution, as discussed in Section 2.3. Our results indicate that aggregated CaCO_3 interact with Fetuin-A proteins to form a complex. After Fetuin-A is combined with CaCO_3 particles, SEM (Fig. 5A,B) shows that the CaCO_3 nanoparticle aggregates have been stabilized by Fetuin-A. As observed in Fig. 5, spherical Fetuin-A begins to adsorb onto the CaCO_3 phase alone. These Fetuin-A/ CaCO_3 complexes show particle sizes ranging from 400-600 nm after a two-day incubation period (Fig. 5 A,B). Interestingly, the rhombohedral morphologies were no longer observed, confirming protein adsorption on the CaCO_3 nanoparticle aggregates.

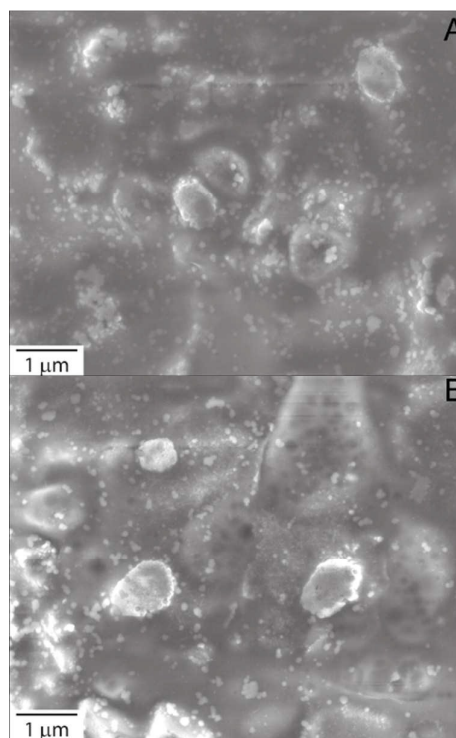


Figure 5. SEM images of Fetuin-A/ CaCO_3 particle-complexes demonstrate the formation of ovoid structure after Fetuin-A stabilization (A,B) in DMEM. Fetuin-A/ CaCO_3 complexes showed different morphological forms, including large and small aggregates.

Future studies will focus on determining the atomic arrangements and possible mechanisms by performing small-angle neutron/X-ray scattering. Previous studies have shown

that calcium carbonate, in the presence of an acidic protein, binds parallel to the calcium plane, resulting in changes in the rhombohedral morphological structure and surface smoothness.⁵⁸ As observed by SEM, The CaCO₃ rhombohedral structures were lost when Fetuin-A/CaCO₃ complexes were formed (Fig. 5A,B), which matches prior literature reports and supports the deaggregation and dissociation of the CaCO₃ particles when Fetuin-A is surrounding the CaCO₃ aggregate.

To examine the morphological changes within the Fetuin-A/CaCO₃ complexes, high-resolution TEM analysis was also conducted. Three interesting morphologies were observed which point to possible stabilization/passivation mechanisms and binding interactions between Fetuin-A and the CaCO₃ nanoparticle structures. First, a corona surrounding unstructured agglomerates of CaCO₃ particles is observed (Fig. 6A) for mature (longer incubation time) Fetuin-A/CaCO₃ complexes, as previously shown by neutron scattering experiments.⁵⁵

A second morphology was observed (Fig. 6B), and is attributed to a transient state in which Fetuin-A proteins are bound to small CaCO₃ particles (Fig. 6B inset) Similar branches with defined orientation have been observed with hydroxyapatite crystals in the presence of special block copolymers.⁶⁰ This second morphological structure can produce more stable Fetuin-A/CaCO₃ complexes with ovoid structure, similar to those observed with SEM and further confirmed with DLS studies (Section 2.3). The third morphology (Fig. 6C) shows the presence of needle-like structures in the corona, a more diffuse core, and small CaCO₃ particles observed at the exterior (Fig. 6C inset). These needle-like structures have been well-reported in the literature for the formation of calcium-protein complexes.⁵² These results can aid in understanding the formation of Fetuin-A/CaCO₃ complexes; for instance, in this study Fetuin-A is shown to induce the formation of calcium-protein complexes with CaCO₃ particles without the presence of phosphate ions as reported elsewhere.^{22, 51, 54} Thus, Fetuin-A also interacts with CaCO₃ in a similar fashion as hydroxyapatite crystals; thus, special considerations should be considered for the development of drug delivery vehicles consisting of CaCO₃ particles.

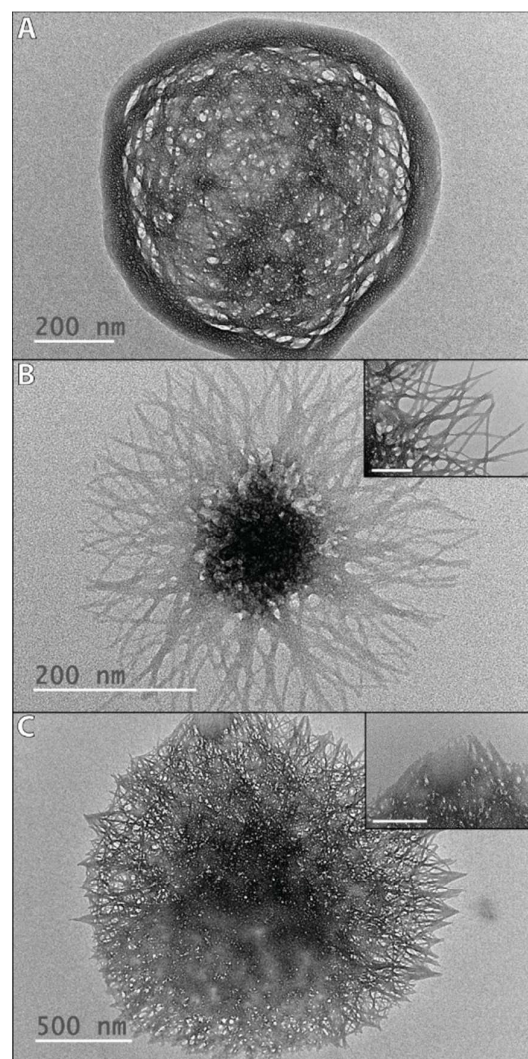


Figure 6. Representative Fetuin-A/CaCO₃ complexes observed under TEM reveals the adsorption and complete surface coverage of Fetuin-A onto CaCO₃. CaCO₃ nanoparticle aggregate cores are stabilized by the surrounding protein shell (A). Possible intermediate forms (B, C) show needle-like structures (inset) formed on the periphery of large CaCO₃ aggregates. These intermediate forms also show calcium nano-sized spheres 'appearing to be removed from the large CaCO₃ core after Fetuin-A adsorption (insets). Scale bars for inset images are 200 nm.

2.3 *In situ* characterization of Fetuin-A/CaCO₃ complexes

Dynamic light scattering (DLS) and UV-Vis spectroscopy were used to analyze the *in situ* hydrodynamic diameter and molecular absorbance of Fetuin-A and the Fetuin-A/CaCO₃ complexes while in an aqueous simulated body fluid (DMEM). A number-averaged particle diameter of 6 ± 0.74 nm was obtained by DLS for Fetuin-A in DMEM (Fig. 7A,C), and compares well with literature measurements of 4.2 nm for Fetuin-A corresponding to an ASHG monomer.¹⁸

Number-averaged mean diameters for these samples were reproducible, as shown by the plots for multiple runs (Fig. 7B). Prior studies on neat Fetuin-A showed that larger agglomerates form in aqueous solutions, and this behavior was observed with our samples. In this study, a few large-sized aggregates were also observed as demonstrated by the high

intensity-low number DLS peaks at higher hydrodynamic diameters (Fig. S4).

Results for the effective particle diameter (using the Stokes-Einstein equation) corroborate the adsorption of Fetuin-A onto the aggregated CaCO_3 structures. Fig. 7A shows an increase in the effective diameter of the CaCO_3 nanoparticle aggregates from the adsorption of the much smaller Fetuin-A. Moreover, changes in zeta potential are indicators of protein adsorption, as discussed elsewhere.⁶¹ For CaCO_3 nanoparticles, a very stable zeta potential of -24.2 ± 1.8 mV was observed. However, after Fetuin-A/ CaCO_3 complexes formation, an increase in surface charge was obtained (-0.1 ± 9 mV), confirming the Fetuin-A adsorption process on CaCO_3 in DMEM.

Interestingly, after an incubation time of four days at ambient temperature and no further mechanical treatment, a decrease in the effective diameter was observed. This size decrease at longer incubation times supports the stabilization of the Fetuin-A/ CaCO_3 complexes⁶² followed by removal of calcium from the interior, as was indicated by TEM (Fig. 6C). Thus, Fetuin-A not only inhibits further growth of the CaCO_3 nanoparticle aggregate, it also potentially aids in the solubilisation and dispersal of the calcite form of CaCO_3 over time (Figs. 7B, and S4). To further confirm this result, a control experiment without Fetuin-A was performed in which DMEM and CaCO_3 particles were incubated for 4 days (Fig. 7B).

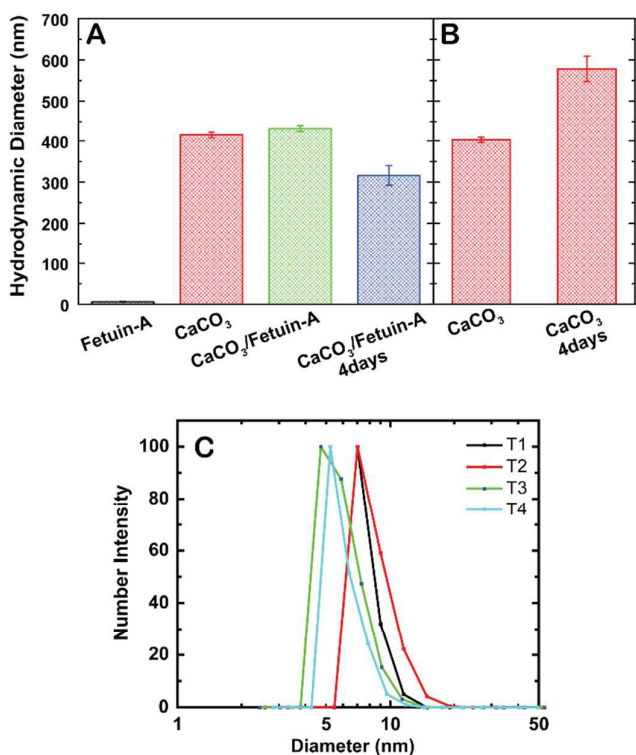


Figure 7. (A) Average effective hydrodynamic diameter increases from the CaCO_3 nanoparticle aggregate to the Fetuin-A/ CaCO_3 complex, confirming the adsorption of Fetuin-A on the surface. After a 4-day (96 h) incubation period, a significant decrease in size was observed (~27%), suggesting the removal of calcium from the complex, as indicated by TEM. (B) Neat CaCO_3 nanoparticles instability in DMEM and significant (43%) increase in size after a 4-day (96 h) incubation period. (C) Number intensity DLS particle size data are shown for neat Fetuin-A indicating stability in DMEM.

Results showed an increase in effective diameter for the CaCO_3 particles when Fetuin-A is not present; therefore, the decrease in CaCO_3 diameter is attributed to the presence of Fetuin-A. Additional control experiments are discussed in ESI 2 (Figs. S4 and S5). UV-Vis spectroscopy has been previously utilized to study the adsorption mechanisms of proteins on different substrates,⁶³ and was used in this study to compare neat CaCO_3 particles to Fetuin-A/ CaCO_3 complexes in solution. The UV-Vis results confirm adsorption of Fetuin-A onto the CaCO_3 particles, as shown by a slight shift in maximum molecular absorbance as compared to neat Fetuin-A (Fig. S6); these results are discussed in more detail in ESI3.

3. Conclusions

In this study, Fetuin-A has been shown to adsorb, stabilize and bind, and chemically and morphologically modify calcium carbonate particles in a simulated body fluid (DMEM). These results are important since calcium carbonate plays a significant role in current drug delivery applications and biomineralization, and is becoming an attractive material for future pharmaceutical and biomedical applications. Results obtained in this study can be used to evaluate the role and impact of Fetuin-A when in the presence of CaCO_3 calcite particles, and extends prior studies on how Fetuin-A affects hydroxyapatite formation. The chemical and physical characterizations of calcite calcium carbonate (CaCO_3), the glycoprotein Fetuin-A, and Fetuin-A/ CaCO_3 complexes provide the basis for further studies examining the functional group involved in short- and long-term interactions. It has been shown that Fetuin-A can stabilize the calcium ions present in CaCO_3 particles without the presence of a phosphate ion, as has been purported elsewhere. The Fetuin-A/ CaCO_3 complexes have been shown to be time-sensitive, with the mechanism including an initial adsorption, followed by a complex stabilization period, and then destabilization and removal of the calciprotein particles. This mechanism has been explored using SEM and TEM to examine the morphological/structural changes, FTIR and XPS for chemical characterization, and DLS, cryo TEM and UV-Vis for *in situ* characterization of the complex formation and evolution. The characterization methods presented in this study can be applied to the study of other protein-substrate interactions, including more commonly studied minerals such as calcium phosphate salts. The results from this study show that Fetuin-A has potential as a native glycoprotein which can be useful in the development of biomedical therapeutics by stabilizing inorganic particles that are currently being explored as drug delivery vehicles.

4. Experimental Section

4.1 Materials

Human Fetuin-A was used as-received and reconstituted to a concentration of 0.1 mg/mL (Sigma-Aldrich, St. Louis, MO; Biovendor, Asheville, NC). After preparation, Dulbecco's modified Eagle's medium (DMEM) (Corning, Lowell, MA) was

filtered prior to use with a cellulose nitrate 0.22 μm pore membrane (Corning) followed by a 0.1 μm Acrodisc® Supor® membrane. By using double filtered, large particles were separated from the fluid media, allowing to characterize only the CaCO_3 nanoparticles. DI water was used from an EMD Millipore Water purification system (Type I reagent grade water). Calcium carbonate (CaCO_3) nanoparticles (15–40 nm) were used as-received and without any further modification (SkySpring Nanomaterials, Inc., TX, USA).

4.2 Fetuin-A/ CaCO_3 nanoparticle complex formation

For the Fetuin-A/ CaCO_3 particles used in this work, DMEM was the solvent for all solutions. After two-stage DMEM filtering procedures, as discussed in the Section 4.1, a small aliquot of DMEM was examined with DLS to guarantee a zero effective diameter and a clean DMEM fluid media for CaCO_3 in-situ studies. Then, a solution with a concentration of 0.1 mg/mL of CaCO_3 in DMEM was prepared (4 mL). This solution was then filtered using an Acrodisc® 1.2 μm Versapor® membrane syringe filter, and sonicated for 5 minutes using a sonication bath (VWR) without heating. After sonication, DLS measurements were performed and the effective diameter of the sample was recorded. Fetuin-A protein (100 μL) was then added, approximately after 15 min after initial CaCO_3 solution preparation, at a concentration of 100 $\mu\text{g/mL}$. This solution containing CaCO_3 and Fetuin-A in DMEM was then studied using DLS, TEM, FTIR, XPS, UV-Vis, and SEM to examine the formation and evolution of the Fetuin-A/ CaCO_3 complexes.

4.3 Chemical Characterization

A Nicolet 6700 FTIR spectrophotometer (Thermo Electron Corporation) with a He-Ne laser, MCT-A* detector, and KBr beamsplitter with a Miracle-ATR™ accessory (Diamond-ZnSe crystal, PIKE Technologies) was used for ATR-FTIR spectra collection. Fetuin-A, CaCO_3 , and Fetuin-A/ CaCO_3 nanoparticle complexes samples were deposited onto the ATR crystal from solution, the solvent was allowed to dry, leaving a thin sample film on the crystal's surface. Infrared spectral data was then collected and analyzed using Omnic software (v8.1.10, 1992–2009, Thermo Fisher Scientific, Inc.), and a minimum of 256 scans collected for each sample. X-ray photoelectron spectroscopy (XPS) was conducted using a PHI 1600 XPS surface analysis system (Physical Electronics, Mg K_{α} X-ray source (300 W, 15 kV), 45° take-off angle, PHI 10-360 spherical capacitor energy analyzer, and an Omni Focus II small-area lens. All samples were deposited from solution onto a clean gold-coated silicon wafer substrate. A total of 10 scans with 26.95 eV pass energy across the 1100–0 eV range were analyzed for survey scans. High-resolution XPS spectra consist of a minimum of 25 scans, at a 23.5 eV pass energy and 0.1 eV step size. At least three spectra per sample were analyzed, and the averages are reported. Data analysis was performed using Origin Pro 2015.

4.4 Morphological Characterization.

Scanning electron microscopy (SEM) was performed using a JEOL JSM-6500 field emission scanning electron microscope (FE-SEM) operated at 5 or 15 keV. Sample preparation was performed in a similar manner to the XPS analysis; however, the gold-coated silicon wafers were mounted on SEM holders using double-sided black carbon tape. High-resolution transmission electron microscopy (TEM) images were obtained using a JEOL 2100 at 200 kV. For TEM, sample droplets were placed on a carbon Formvar Cu grid 300 mesh (Electron Microscopy Science), and the liquid was evaporated at ambient conditions inside a fume hood. Cryo TEM images were collected using a JEOL 1400 Biological TEM with a Gatan Cryoplunge™ adapter.

4.5 Particle Diameters

Dynamic light scattering (DLS) and zeta-potential phase-angle light scattering (PALS) measurements were conducted using a ZetaPALS instrument (659 nm wavelength, 90° detector, Brookhaven Instruments Corporation (BIC), Holtsville, NY). At least 5 measurements were taken for each sample, including 30 measurement cycles for each PALS experiment. Outlier analysis was performed at a 0.05 level of significance using Grubb's test. Samples were analyzed at ambient temperature conditions (~22 °C). Results reported are based on Stokes-Einstein equation for the effective hydrodynamic diameter, or average mean diameter by number, and is specified for each analysis.

4.6 Protein Adsorption Studies

A Shimadzu 2550 UV-Vis spectrometer was utilized for the analysis of the Fetuin-A glycoprotein and its adsorption onto aggregated calcium carbonate nanoparticles. Filtered DMEM was used as the blank.

Acknowledgements

This work was funded by the National Science Foundation (EPS-0903787; IIA-1430364) and the Mississippi INBRE (IDEA Network for Biomedical Research Excellence). DLS and TEM instrumentation was provided by NSF grants EPS-0903787 and DBI-1126743, respectively. We are very grateful to Ying Xiao and Dr. Clayton Loehn at Louisiana State University for assisting in some of the TEM work presented in this study, and to Dr. I-Wei Chu at Institute for Imaging and Technical Technologies (I2AT) at Mississippi State University for her assistance with some of the SEM and TEM imaging.

References

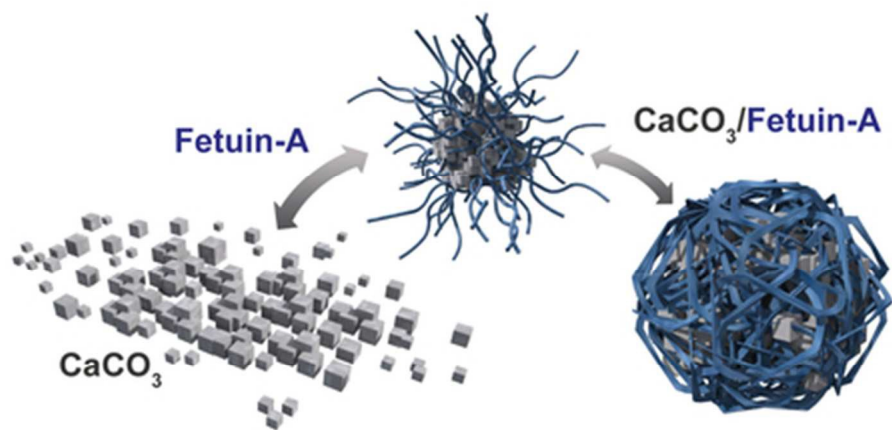
1. S. K. L. Levengood and M. Zhang, *Journal of Materials Chemistry B*, 2014, **2**, 3161–3184.
2. L. K. Grunenfelder, N. Suksangpanya, C. Salinas, G. Milliron, N. Yaraghi, S. Herrera, K. Evans-Lutterodt, S. R. Nutt, P. Zavattieri and D. Kisailus, *Acta Biomaterialia*, 2014, **10**, 3997–4008.

3. E. S. Vasquez, I. W. Chu and K. B. Walters, *Langmuir*, 2014, **30**, 6858-6866.
4. J. Sun, C. Chen, H. Pan, Y. Chen, C. Mao, W. Wang, R. Tang and X. Gu, *Journal of Materials Chemistry B*, 2014, **2**, 4544-4553.
5. A. Schulz, H. Wang, P. van Rijn and A. Boker, *Journal of Materials Chemistry*, 2011, **21**, 18903-18918.
6. M. W. Trim, M. F. Horstemeyer, H. Rhee, H. El Kadiri, L. N. Williams, J. Liao, K. B. Walters, J. McKittrick and S.-J. Park, *Acta Biomaterialia*, 2011, **7**, 1228-1240.
7. L. K. Grunenfelder, S. Herrera and D. Kisailus, *Small*, 2014, **10**, 3207-3232.
8. C. Tan, Z. Sun, Y. Hong, Y. Li, X. Chen and X. Zhang, *Journal of Materials Chemistry B*, 2013, **1**, 3694-3704.
9. D. Wei, W. Xiao, J. Sun, M. Zhong, L. Guo, H. Fan and X. Zhang, *Journal of Materials Chemistry B*, 2015, **3**, 2753-2763.
10. E. Abdullayev and Y. Lvov, *Journal of Materials Chemistry B*, 2013, **1**, 2894-2903.
11. Q. Ruan and J. Moradian-Oldak, *Journal of Materials Chemistry B*, 2015, DOI: 10.1039/C5TB00163C.
12. L. L. Demer and Y. Tintut, *Circulation*, 2008, **117**, 2938-2948.
13. X. Wang, C. Wu, K. Tao, K. Zhao, J. Wang, H. Xu, D. Xia, H. Shan and J. R. Lu, *The Journal of Physical Chemistry B*, 2010, **114**, 5301-5308.
14. R. K. DeLong, C. M. Reynolds, Y. Malcolm, A. Schaeffer, T. Severs and A. Wanekaya, *Nanotechnology, Science and Applications*, 2010, **3**, 53-63.
15. W. Zhu, J. Lin, C. Cai and Y. Lu, *Journal of Materials Chemistry B*, 2013, **1**, 841-849.
16. J. Lee and H.-s. Yun, *Journal of Materials Chemistry B*, 2014, **2**, 1255-1263.
17. Y. Yamamoto, T. Nishimura, A. Sugawara, H. Inoue, H. Nagasawa and T. Kato, *Crystal Growth & Design*, 2008, **8**, 4062-4065.
18. A. Heiss, A. DuChesne, B. Denecke, J. Grötzinger, K. Yamamoto, T. Renneé and W. Jahnen-Dechent, *Journal of Biological Chemistry*, 2003, **278**, 13333-13341.
19. W. Jahnen-Dechent, C. Schäfer, M. Ketteler and M. McKee, *J Mol Med*, 2008, **86**, 379-389.
20. V. Persy and P. D'Haese, *Trends in Molecular Medicine*, 2009, **15**, 405-416.
21. A. Pasch, S. Farese, S. Graber, J. Wald, W. Richtering, J. Floege and W. Jahnen-Dechent, *Journal of the American Society of Nephrology : JASN*, 2012, **23**, 1744-1752.
22. J. Wald, S. Wiese, T. Eckert, W. Jahnen-Dechent, W. Richtering and A. Heiss, *Soft Matter*, 2011, **7**, 2869-2874.
23. M.-Q. Gong, J.-L. Wu, B. Chen, R.-X. Zhuo and S.-X. Cheng, *Langmuir*, 2015, **31**, 5115-5122.
24. C. Qi, Y.-J. Zhu and F. Chen, *ACS Applied Materials & Interfaces*, 2014, **6**, 4310-4320.
25. W. Wei, G.-H. Ma, G. Hu, D. Yu, T. McLeish, Z.-G. Su and Z.-Y. Shen, *Journal of the American Chemical Society*, 2008, **130**, 15808-15810.
26. L. Brylka and W. Jahnen-Dechent, *Calcified tissue international*, 2013, **93**, 355-364.
27. M. Mihai, F. Bucătariu, M. Aflori and S. Schwarz, *Journal of Crystal Growth*, 2012, **351**, 23-31.
28. A. Haglund, B. Ek and P. Ek, *Biochem. J.*, 2001, **357**, 437-445.
29. J. T. Lee, Y. Leng, K. L. Chow, F. Ren, X. Ge, K. Wang and X. Lu, *Acta Biomater*, 2011, **7**, 2615-2622.
30. T. Kokubo and H. Takadama, *Biomaterials*, 2006, **27**, 2907-2915.
31. A. C. Tas, *Acta Biomaterialia*, 2014, **10**, 1771-1792.
32. E. Foran, S. Weiner and M. Fine, *Sci. Rep.*, 2013, **3**.
33. J. D. Rodriguez-Blanco, S. Shaw and L. G. Benning, *Nanoscale*, 2011, **3**, 265-271.
34. M. A. Legodi, D. de Waal, J. H. Potgieter and S. S. Potgieter, *Minerals Engineering*, 2001, **14**, 1107-1111.
35. Z. Ganim, H. S. Chung, A. W. Smith, L. P. DeFlores, K. C. Jones and A. Tokmakoff, *Accounts Chem. Res.*, 2008, **41**, 432-441.
36. A. Barth, *Biochimica et Biophysica Acta (BBA) - Bioenergetics*, 2007, **1767**, 1073-1101.
37. G. Steiner, S. Tunc, M. Maitz and R. Salzer, *Anal Chem*, 2007, **79**, 1311-1316.
38. R. Podila, R. Chen, P. C. Ke, J. M. Brown and A. M. Rao, *Appl Phys Lett*, 2012, **101**, 263701.
39. M. M. Patel, J. D. Smart, T. G. Nevell, R. J. Ewen, P. J. Eaton and J. Tsibouklis, *Biomacromolecules*, 2003, **4**, 1184-1190.
40. C. Gruian, E. Vanea, S. Simon and V. Simon, *Biochimica et Biophysica Acta (BBA) - Proteins and Proteomics*, 2012, **1824**, 873-881.
41. T. L. Barr and S. Seal, *Journal of Vacuum Science & Technology A*, 1995, **13**, 1239-1246.
42. S. L. Stipp and M. F. Hochella Jr, *Geochimica et Cosmochimica Acta*, 1991, **55**, 1723-1736.
43. W. J. Landis and J. R. Martin, *Journal of Vacuum Science & Technology A*, 1984, **2**, 1108-1111.
44. T. L. Barr and S. Seal, *Journal of Vacuum Science & Technology A*, 1995, **13**, 1239-1246.
45. B. G. Russell, W. E. Moddeman, J. C. Birkbeck, S. E. Wright, D. S. Millington, R. D. Stevens and K. E. Dombrowski, *Biospectroscopy*, 1998, **4**, 257-266.
46. S. Ray and A. G. Shard, *Anal Chem*, 2011, **83**, 8659-8666.
47. E. Vanea, K. Magyari and V. Simon, *Journal of Optoelectronics and Advanced Materials*, 2010, **12**, 1206.
48. L. D. Setiawan, H. Baumann and D. Gribbin, *Surf Interface Anal*, 1985, **7**, 188-195.
49. I. Carvalho, R. E. Galindo, M. Henriques, C. Palacio and S. Carvalho, *Journal of Physics D: Applied Physics*, 2014, **47**, 335401.
50. N. A. J. M. Sommerdijk and G. d. With, *Chemical Reviews*, 2008, **108**, 4499-4550.
51. A. Heiss, W. Jahnen-Dechent, H. Endo and D. Schwahn, *Biointerphases*, 2007, **2**, 16-20.
52. A. Heiss, T. Eckert, A. Aretz, W. Richtering, W. Van Dorp, C. Schäfer and W. Jahnen-Dechent, *Journal of Biological Chemistry*, 2008, **283**, 14815-14825.
53. P. A. Price, G. R. Thomas, A. W. Pardini, W. F. Figueira, J. M. Caputo and M. K. Williamson, *J Biol Chem*, 2002, **277**, 3926-3934.
54. K. Mori, M. Emoto and M. Inaba, *Recent Patents on Endocrine, Metabolic and Immune Drug Discovery*, 2011, **5**, 124-146.
55. W. Jahnen-Dechent, A. Heiss, C. Schafer and M. Ketteler, *Circ Res*, 2011, **108**, 1494-1509.
56. L. B. Gower, *Chemical Reviews*, 2008, **108**, 4551-4627.
57. F. Nudelman, K. Pieterse, A. George, P. H. H. Bomans, H. Friedrich, L. J. Brylka, P. A. J. Hilbers, G. de With and N. A. J. M. Sommerdijk, *Nat Mater*, 2010, **9**, 1004-1009.
58. L. Addadi and S. Weiner, *Proceedings of the National Academy of Sciences*, 1985, **82**, 4110-4114.
59. L. Gago-Duport, M. J. I. Briones, J. B. Rodríguez and B. Covelo, *Journal of structural biology*, 2008, **162**, 422-435.
60. Q. Zhang, S.-J. Liu and S.-H. Yu, *Journal of Materials Chemistry*, 2009, **19**, 191-207.

Paper

Journal of Materials Chemistry B

61. K. Rezwani, A. R. Studart, J. Vörös and L. J. Gauckler, *The Journal of Physical Chemistry B*, 2005, **109**, 14469-14474.
62. P. A. Price and J. E. Lim, *Journal of Biological Chemistry*, 2003, **278**, 22144-22152.
63. K. Siriwardana, M. Gadogbe, S. M. Ansar, E. S. Vasquez, W. E. Collier, S. Zou, K. B. Walters and D. Zhang, *The Journal of Physical Chemistry C*, 2014, **118**, 11111-11119.



Fetuin-A adsorbs and stabilizes calcite CaCO_3 , as indicated by chemical and morphology changes. Complexed Fetuin-A/ CaCO_3 showed time-dependent changes in structure in a simulated body fluid. Fetuin-A is an agent capable of inhibiting, and possibly solubilizing calcium carbonate particulates, as shown by decreased complex size over time.

39x19mm (300 x 300 DPI)

39x19mm (300 x 300 DPI)